Article
Vol. 23, No. 1, p. 165–174, February 2019
https://doi.org/10.1007/s12303-018-0008-1
pISSN 1226-4806 eISSN 1598-7477
Geosciences Journal GJ

A new model for predicting surface mining subsidence: the improved lognormal function model

Weitao Yan[1,2]*, Junjie Chen[1], and Yueguan Yan[2]

[1]School of Surveying and Land Information Engineering, Henan Polytechnic University, Jiaozuo, Henan 454003, China
[2]College of Geoscience and Surveying Engineering, China University of Mining and Technology Beijing, Xueyuan Road D11, Haidian District, Beijing 100083, China

ABSTRACT: Mining-induced problems in the coal field seriously threaten the normal operation of the mines and cause significant property losses and environmental disruption. Thus, high precision subsidence prediction is important on the processing of mining subsidence problems. In this paper, we analyzed the formation mechanism of skewed subsidence. The rock beam on the side of the gob and coal pillar presented different supporting reaction force, and the difference resulted in the asymmetric distribution of subsidence velocity, which further led to the formation of the surface skewed subsidence basin. The relationship between the wave curve and vibration curve was determined, and the skewed subsidence process of the surface point in the mining affected area was analyzed. The total duration of the initial and accelerated subsidence phases is smaller than that of the decelerated and end subsidence phases. Then, from the skewed subsidence characteristics, the skewed subsidence prediction model based on the lognormal function was built. An application example was selected to validate the feasibility and effectiveness of the proposed model. Results showed that the model has good prediction ability.

Key words: surface mining subsidence, skewed prediction model, lognormal function

Manuscript received September 12, 2017; Manuscript accepted February 23, 2018

1. INTRODUCTION

In recent years, the rapid growth of China's economy has led to the consumption of substantial resources. Coal resource accounts for nearly 70% of the primary energy structure in China. With the intensive growth of underground coal mining industry, the ecology and environment of mining area have been seriously disturbed and destroyed, and the safe use of buildings, railways and highways have also been seriously affected (Zhang et al., 2012; Cui et al., 2014). Mining-induced problems, such as economic (Sinha et al., 2007), ecological and environmental problem (Bell et al., 2000; Wang et al., 2010; Saha et al., 2011; Fan et al., 2015), have seriously affected the sustainable development of mining area and people's normal lives. Implementing subsidence control projects can greatly reduce or mitigate surface damages and assist in the development of a harmonious society. Furthermore, studies of mining subsidence laws and mining subsidence prediction methods are regarded as important research fields in subsidence control engineering. Therefore, consolidating these mining subsidence laws and research of mining subsidence prediction methods has important practical application value.

Mining subsidence is an integrated mechanical evolution process, and its subsidence mechanism is complex and changeable. The main factors that affect the subsidence law are mining thickness (Ma et al., 2012; Yu et al., 2015), mining depth (Xuan et al., 2008; Fan et al., 2011; Wang et al., 2012; Ju et al., 2015; Wang et al., 2015; Lu et al., 2016; Salmi et al., 2017), dip angle of coal seam (Hiramatsu et al., 1989; Ren et al., 1989; Luo et al., 2009), lithology (Sasaoka et al., 2015), mining adequacy (Dai et al., 2003), topographic conditions (Holla et al., 1997; Dai et al., 2000; Tang et al., 2009), roof management method and mining method (He et al., 1991). Surface subsidence requires different laws depending on the type of geological and mining condition. In simple flat terrain condition, it is usually considered that the surface subsidence basin induced by the critical mining of horizontal coal seams is symmetrically distributed at the center of the mined out area. From this symmetrical distribution characteristic of the subsidence basin, some subsidence laws were systematically studied. For

*Corresponding author:
Weitao Yan
School of Surveying and Land Information Engineering, Henan Polytechnic University, Jiaozuo, Henan 454003, China
Tel: +86-13051610335, E-mail: yanweitao2008@163.com

example, maximum subsidence occurs near the central top part of the gob, and maximum horizontal movement occurs above the boundary of the mining area, among other laws (Peng et al., 1978; Kratzsch et al., 1983). These subsidence laws were applied to engineering practice, and some achievements were obtained. However, an analysis of many examples suggested that surface subsidence basins do not strictly follow symmetrical distributions, and thus, the skewed distribution mechanisms and characteristics of surface subsidence basins were analyzed by some scholars (Wang et al., 1999). Some researchers found that the bedrocks are broken in the "cantilever beam" structure on the working face side, and is broken in the "clamped beam" structure on the open-off cut side. This difference results in the asymmetry of overlying fractures, which then leads to the formation of a surface skewed subsidence basin.

At present, the commonly used methods for mining subsidence prediction include the section function method, influence function method, typical curve method, and theory and numerical method, among others. The probability integration method is a type of influence function method that has been accepted and widely used in China. The probability integral method is based on the stochastic medium theory and the superposition principle, and its function form is in line with the normal distribution function. The symmetric distribution characteristic of the probability integration method cannot fully reflect the skewed distribution of surface subsidence basins when the probability integral method is used to predict subsidence, and thus, the error is relatively large. A skewed subsidence prediction model based on the lognormal distribution function is therefore proposed to effectively predict mining subsidence in line with the mechanism analysis of skewed subsidence. Combined with the example used in this study, the skewed characteristic of the surface point subsidence and the reliability of the prediction model are both analyzed and verified.

2. EXPERIMENTAL REGION AND MONITORING DATA

The Shendong coal field is located at the contiguous part of Inner Mongolia and Shaanxi Province and in the border area of the Loess Plateau and the Mu Us Desert. Rich coal resources exist in this area and correspond to China's first hundred million tons of coal production base. The mining features in this area can be described as having shallow-buried depth, thin bedrock, thick loose layers, large mining height and fast mining velocity. Working face 407 belongs to the Halagou mine with an average thickness, depth and dip angle of 5.2 m, 130 m and 1°, respectively. The size of the working face 407 is 3,224 m × 284 m. The bedrock thickness is 73 m, the alluvium thickness is 57 m, and the aquifer thickness is 10–24 m. According to mining conditions and borehole histogram of working face 407, the lithology of the overlying strata in this working face is evaluated as medium hard. The method of comprehensive mechanized coal mining is used and all caving methods are adopted for roof management. The average advance velocity is 15 m/day. The observation lines along the strike and dip direction were laid out above the working face 407 (Fig. 1). The spacing of the observation stations is 15 m.

Point A12, A13 and A14 are located in the full subsidence area,

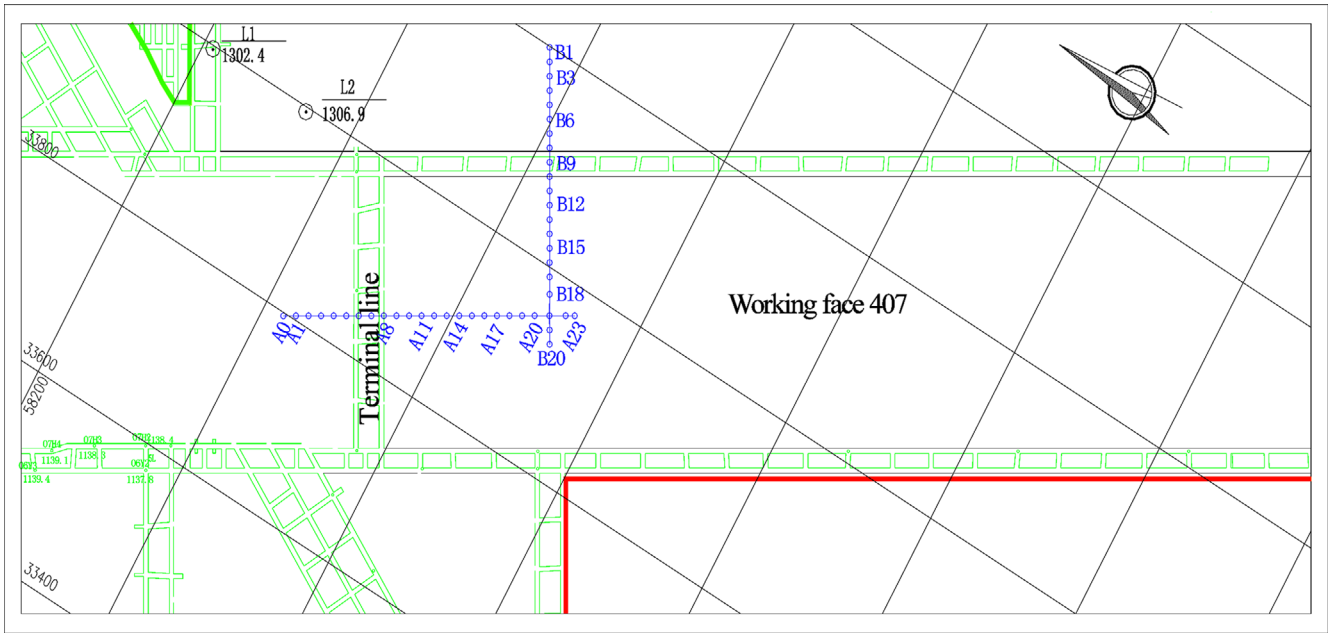

Fig. 1. Layout of ground observation stations.

Table 1. Monitoring data of surface point

Date	Monitoring time (day)	Cumulative Subsidence value of point A14 (mm)	Cumulative Subsidence value of point A13 (mm)	Cumulative Subsidence value of point A12 (mm)
2013-11-12	1	0	0	0
2013-12-31	49	22.0	30	10
2014-01-05	54	138.5	72.5	46.5
2014-01-07	56	802.5	481.5	379.5
2014-01-09	58	2203.5	1721.5	1576.5
2014-01-11	60	2911.5	2720.5	2286.5
2014-01-13	62	2956.5	2817.5	2405.5
2014-05-29	198	3191.5	3082.5	3061.5
2014-05-30	199	3201.5	3092.5	3071.5
2014-05-31	200	3206.5	3097.5	3075.5
2014-09-25	317	3220.0	3111.5	3090.5
2014-09-27	319	3220.5	3111.5	3090.5

and its movement and deformation are fully developed. Therefore, this point were selected for the analysis of the subsidence law of the monitoring point and the applicability of the skewed prediction function. Point A12, A13 and A14 were in-suit monitored 12 times. The monitoring information is shown in the Table 1.

3. SKEWED SUBSIDENCE CHARACTERISTICS OF THE ROCK MASS

3.1. Model Selection and Construction of the Coordinate System

Based on the experimental and research results of Liu (1982) and Ramesh (1995), the coal seam and overlying strata belong to the viscoelastic rock mass category, and are in line with the Kelvin rheological model (Fig. 2).

The constitutive equation of the Kelvin rheological model is as follows (Liu, 1982):

$$\sigma = E\varepsilon + \eta\dot{\varepsilon}, \tag{1}$$

where σ and ε denote stress and strain, respectively; E is the elasticity modulus; η is the viscosity coefficient; and $\dot{\varepsilon} = d\varepsilon/dt$ is the change rate of strain.

To simplify the model, we reduced the model parameters, and improved the running speed and applicability of the model by considering the following assumptions (Liu, 1982):

(1) The strata are bedded and horizontally distributed, and the mined out area of the coal seam is a rectangular shape;

(2) The coal seam and overlying strata are in line with the Kelvin rheological model;

(3) No large geological structure exists in the mining area range, and no large geological events occur;

(4) The extraction rate of the coal seam is not considered; and

(5) The initial vertical stress of the rock mass is calculated by Formula (2):

$$P_z = \gamma H, \tag{2}$$

where P_z is the initial vertical stress; γ is the bulk density of the rock mass; and H is the buried depth of the strata.

Figure 3 shows the coordinate system, which can be used for

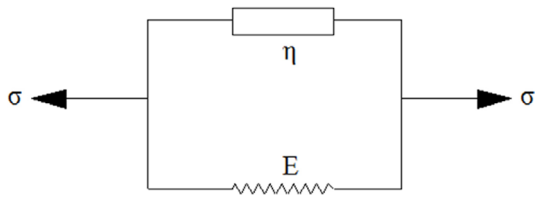

Fig. 2. Kelvin rheological model.

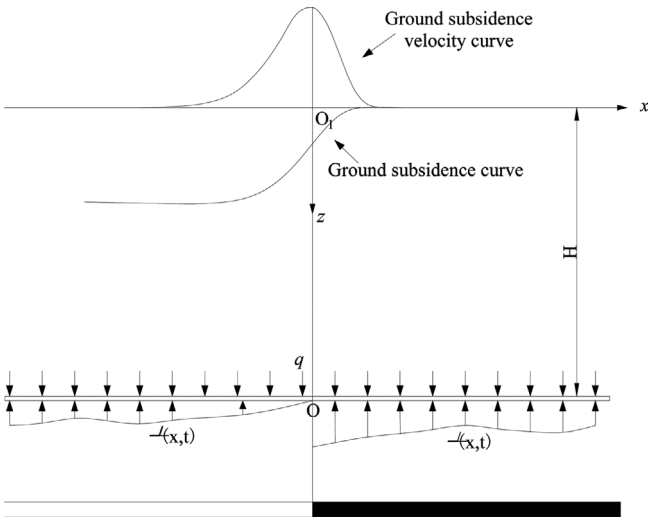

Fig. 3. Construction of coordinate system.

https://doi.org/10.1007/s12303-018-0008-1

the analysis of the subsidence characteristics of the rock mass. First, we set the x axis along the central axis of rock beam. We also considered the part above the pillar as positive and the part above the gob as negative. Then, we set the z axis in the vertical direction, and we considered the downward direction as positive. Finally, we selected the coordinate origin point O is near the top part of gob boundary. Correspondingly, the ground coordinate system XO_1W was established for the earth's surface.

3.2. Spatial Skewed Characteristics of the Surface Subsidence Basin

According to the results of Liu (1982), we can derive the deflection equation of the beam as:

$$W_1(x,t)=\frac{MP_z}{E_k}\frac{L_p^2}{L_k^2}(1-e^{-kt})e^{-\frac{\pi}{L_p}x}\left[-\frac{L_k-L_p}{L_k+L_p}\sin\left(\frac{\pi}{L_p}x\right)+\cos\left(\frac{\pi}{L_p}x\right)\right]+\frac{MP_z}{E_p}\quad x>0,$$

$$W_2(x,t)=\frac{MP_z}{E_k}(1-e^{-kt})\left\{e^{\frac{\pi}{L_k}x}\left[\frac{L_k-L_p}{L_k+L_p}\sin\left(\frac{\pi}{L_k}x\right)-\cos\left(\frac{\pi}{L_k}x\right)\right]+1+\frac{L_p^2}{L_k^2}\right\}+\frac{MP_z}{E_p}\quad x<0, \tag{3}$$

where M is the mining height; E_p and E_k denote the elastic modulus of the coal pillar side and the gob side, respectively, and L_P, L_k is the half wavelength of pressure wave of the coal pillar side and the gob side, respectively.

By calculating the partial derivative of t for $W(x,t)$, the subsidence velocity $v(x,t)$ of each point can be obtained.

When $x>0$,

$$v_1(x,t)=\frac{\partial W_1(x,t)}{\partial t}=ke^{-kt}e^{-\frac{\pi}{L_p}x}\frac{MP_z}{E_k}\frac{L_p^2}{L_k^2}\left[-\frac{L_k-L_p}{L_k+L_p}\sin\left(\frac{\pi}{L_p}x\right)+\cos\left(\frac{\pi}{L_p}x\right)\right]. \tag{4}$$

When $x<0$,

$$v_2(x,t)=\frac{\partial W_2(x,t)}{\partial t}=ke^{-kt}\frac{MP_z}{E_k}\left\{e^{\frac{\pi}{L_k}x}\left[\frac{L_k-L_p}{L_k+L_p}\sin\left(\frac{\pi}{L_k}x\right)-\cos\left(\frac{\pi}{L_k}x\right)\right]+1+\frac{L_p^2}{L_k^2}\right\}. \tag{5}$$

And then, we calculate the partial derivative of x for $v(x,t)$, to derive the the change rate of subsidence velocity along the X axis.

When $x>0$,

$$\frac{\partial v_1(x,t)}{\partial x}=\frac{\partial^2 W_1(x,t)}{\partial t\partial x}=-\frac{\pi}{L_p}ke^{-kt}e^{-\frac{\pi}{L_p}x}\frac{MP_z}{E_k}\frac{L_p^2}{L_k^2}\left[-\frac{L_k-L_p}{L_k+L_p}\sin\left(\frac{\pi}{L_p}x\right)+\cos\left(\frac{\pi}{L_p}x\right)\right]$$

$$+ke^{-kt}e^{-\frac{\pi}{L_p}x}\frac{MP_z}{E_k}\frac{L_p^2}{L_k^2}\left[-\frac{L_k-L_p}{L_k+L_p}\cos\left(\frac{\pi}{L_p}x\right)\frac{\pi}{L_p}-\frac{\pi}{L_p}\sin\left(\frac{\pi}{L_p}x\right)\right]. \tag{6}$$

When $x<0$,

$$\frac{\partial v_2(x,t)}{\partial x}=\frac{\partial^2 W_2(x,t)}{\partial t\partial x}=ke^{-kt}\frac{MP_z}{E_k}\frac{\pi}{L_k}e^{\frac{\pi}{L_k}x}\left[\frac{L_k-L_p}{L_k+L_p}\sin\left(\frac{\pi}{L_k}x\right)-\cos\left(\frac{\pi}{L_k}x\right)\right]$$

$$+ke^{-kt}\frac{MP_z}{E_k}\frac{\pi}{L_k}e^{\frac{\pi}{L_p}x}\left[\frac{L_k-L_p}{L_k+L_p}\cos\left(\frac{\pi}{L_k}x\right)+\sin\left(\frac{\pi}{L_k}x\right)\right]. \tag{7}$$

Given that the strength of the backfill material is smaller than the coal pillar, the following relations can be obtained.

$$E_k<E_p. \tag{8}$$

According to Liu (1982), the formula to calculate L_p and L_k is

$$\begin{cases}L_p=\dfrac{\pi}{\sqrt[4]{\dfrac{E_p}{4IE_bM}}},\\[2ex] L_k=\dfrac{\pi}{\sqrt[4]{\dfrac{E_k}{4IE_bM}}},\end{cases} \tag{9}$$

where I is the moment of inertia of an area, and E_b is the elastic modulus of the beam.

By substituting Formula (8) into Formula (9), we can derive the following relationship:

$$L_p<L_k. \tag{10}$$

By substituting Formulas (8) and (10) into Formulas (6) and (7), we can derive the following relationship:

$$\left|\frac{\partial v_1(x,t)}{\partial x}\right|>\left|\frac{\partial v_2(x,t)}{\partial x}\right|. \tag{11}$$

By Equation (11), we found the change rate of the subsidence velocity along the X axis above the coal pillar is larger than that above the gob. Thus, the subsidence velocity curve of the coal pillar side is steeper, the subsidence velocity curve of the gob side is gentler, and the subsidence curve is not antisymmetrically distributed at the inflection point.

The bend and subsidence of the roof rock leads to the

subsidence of the ground surface. The shapes of the surface subsidence curve and the surface subsidence velocity curve are similar to those of the roof rock. Thus, the subsidence velocity curve of the coal pillar side is steeper than that of the gob side, and the ground surface subsidence curve is also not antisymmetrically distributed at the inflection point (Fig. 3).

3.3. Temporal Skewed Characteristics of the Surface Point Subsidence

In physics, a wave curve corresponds to the vibration distribution law of many particles at a given moment in space domain, and a vibration curve corresponds to the vibration distribution law of a single particle in time domain. For example, as shown in Figure 4, the wave curve propagates forward along the positive direction of the X axis in the form of a sine wave. The fluctuation positions of each particle at the moment t = 0 are shown in the Figure 4a. At t = 0, point A is just affected. Figure 4b presents the vibration curve of point A on the basis of wave theory. A comparison of Figure 4a with Figure 4b shows that the wave curve and the vibration curve are symmetrical.

The relationship between the spatial distribution of the surface subsidence velocity and the time distribution of the single ground point subsidence velocity, is similar to that between the wave and the vibration curve. Thus, the subsidence velocity curve of the single surface point in time domain is symmetrical to that of the ground surface in space domain. From the previous

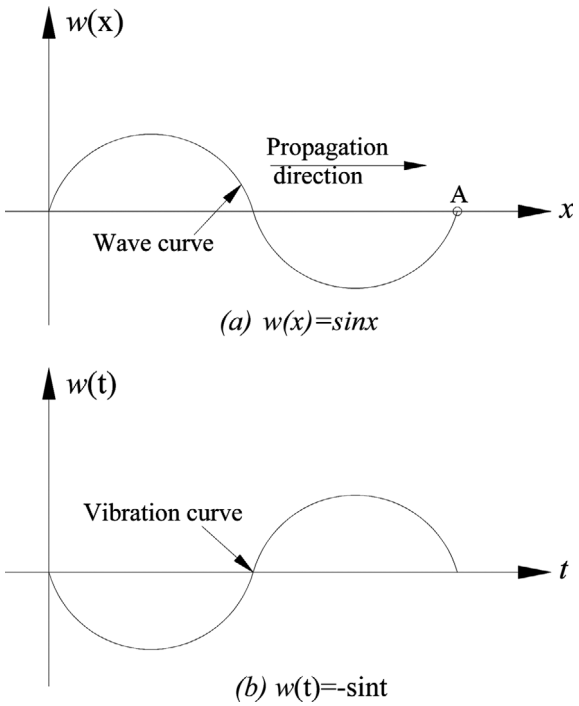

Fig. 4. Wave curve and vibration curve.

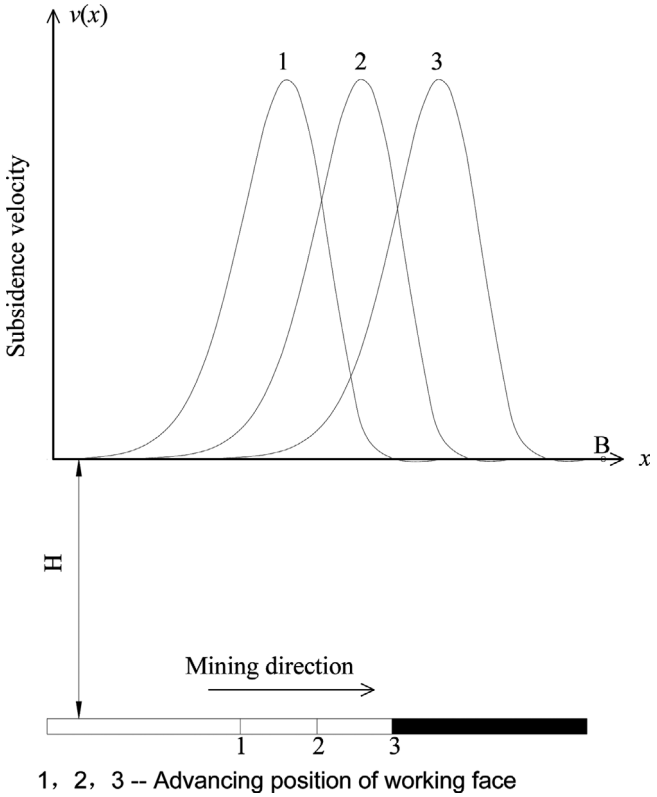

Fig. 5. Surface subsidence velocity curve.

section, we concluded that the subsidence velocity curve is asymmetrically distributed along the mining direction of the working face. Furthermore, the subsidence velocity curve of the coal pillar side is steeper than that of the gob side. With the continuous mining of the coal seam, the asymmetric subsidence velocity curve propagates forward along the mining direction of the working face (Fig. 5).

The magnitude of surface subsidence velocity can reflect surface movement intensity. Therefore, by considering the magnitude of the surface subsidence velocity and its influence on the buildings, the whole movement process of the ground point can be divided into four stages, namely, initial, accelerated, decelerated and end subsidence phases.

- Initial subsidence phase. From the onset movement of the surface to the time when subsidence velocity reaches 1.67 mm/day or 50 mm/month. Which corresponds to stage I in Figure 6.
- Accelerated subsidence phase. Time interval from the time when subsidence velocity reaches 1.67 mm/day to the time when subsidence velocity reaches the maximum value. Which corresponds to stage II in Figure 6.
- Decelerated subsidence phase. Time interval from the time when subsidence velocity reaches the maximum value until surface movement decreases to 1.67 mm/day. Which corresponds to stage III in Figure 6.

https://doi.org/10.1007/s12303-018-0008-1

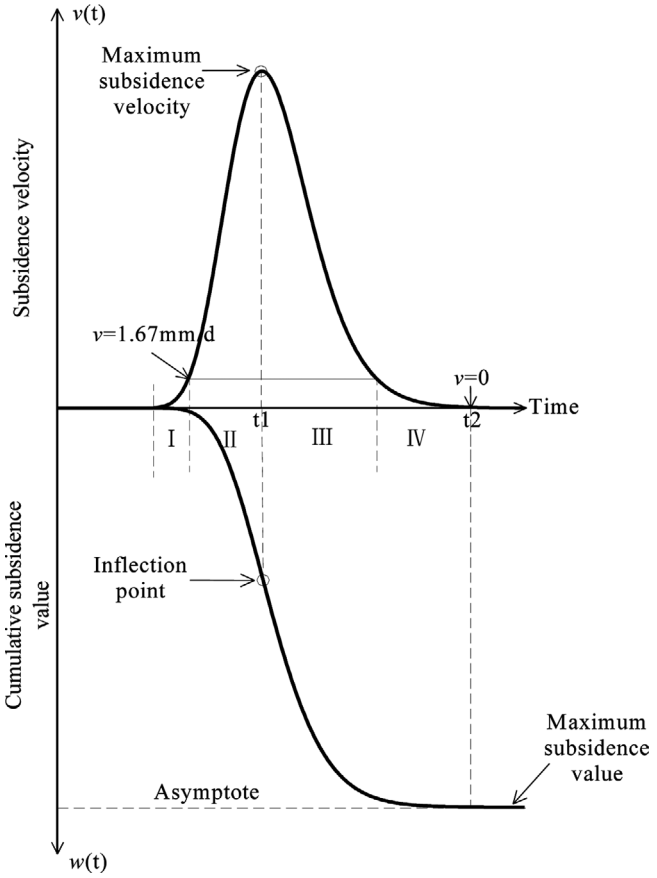

Fig. 6. Skewed subsidence characteristics of subsidence curve and subsidence velocity curve.

- End subsidence phase. From the time when surface movement decreases to 1.67 mm/day to the time when subsidence ends. Which corresponds to stage IV in Figure 6.

As shown in Figure 6, the total duration of the initial and accelerated subsidence phases is smaller than that of the decelerated and end subsidence phases. The subsidence curve and subsidence velocity curve of the initial and accelerated subsidence phases are steep, while the subsidence curve and subsidence velocity curve of decelerated and end subsidence phases is gentle. Thus, the subsidence velocity curve is asymmetric at the maximum value, and the subsidence curve is not antisymmetric at the inflection point.

4. PREDICTION MODEL BASED ON THE LOGNORMAL FUNCTION

4.1. Establishment of the Prediction Model

The probability density function and cumulative distribution function of the lognormal function is expressed by the following equations:

$$f(x) = \begin{cases} \frac{1}{\sqrt{2\pi}\sigma x}\exp\left[-\left(\frac{\ln x-\mu}{\sqrt{2}\sigma}\right)^2\right] & x>0, \\ 0 & x\le 0, \end{cases} \tag{12}$$

$$F(x) = \frac{1}{2}+\frac{1}{2}erf\left[\frac{\ln x-\mu}{\sqrt{2}\sigma}\right], \tag{13}$$

where μ is the expected value of ln x; σ is the standard deviation of ln(x); x is the independent variable; $f(x)$ is the probability density function; and $F(x)$ is the cumulative distribution function.

We previously established the characteristics of the subsidence velocity and subsidence curves. Accordingly, the subsidence velocity curve of the surface point in the mining affected area are exhibits a right skewed distribution (Fig. 6). The lognormal density function is right skewed distribution. On this basis, the improved skewed prediction model based on the lognormal distribution function is proposed.

The improved subsidence velocity prediction model is

$$v(t) = \frac{w_o}{\sqrt{\pi}Bt}\exp\left[-\left(\frac{\ln t-A}{B}\right)^2\right], \tag{14}$$

where t is monitoring time; w_o is the maximum subsidence value; A is a positional parameter; and B is a shape parameter.

The improved cumulative subsidence prediction model is:

$$w(x) = w_o\left(\frac{1}{2}+\frac{1}{2}\times erf\left(\frac{(\ln t-A)}{B}\right)\right). \tag{15}$$

4.2. Model Parameters and Mathematical Characteristics

We set A as the positional parameter. $t = e^A$ as the moment in which the slope of subsidence curve and subsidence velocity reach the maximum value. And B was set as the shape parameter, i.e., the greater the absolute value of B, the smoother the subsidence velocity curve and subsidence curve will be.

The subsidence velocity value of the surface point initially increases and then decreases after reaching the maximum. When $t < e^A$, the acceleration of subsidence velocity curve is greater than 0 and represented by the upward-concave curve. At $t = e^A$, the acceleration of the subsidence velocity curve is 0 and thus has reached the maximum value. When $t > e^A$, the acceleration of subsidence velocity curve is smaller than 0 and represented by the is downward-convex curve.

The cumulative subsidence curve is a monotonically increasing curve. When $t < e^A$, the subsidence curve is in an upward convex, which represent deformation is in the accelerating stage. At $t = e^A$, the slope of the subsidence curve has reached its maximum value. When $t > e^A$, the subsidence curve is in a downward convex, which represent deformation is in the decelerating stage.

4.3. Accuracy Analysis of the Prediction Model

The model parameters can be derived by applying the least-square principle to the nonlinear curve fitting in-suit data. On the basis of the development trend of the above curve, the values of subsidence and subsidence velocity at the monitoring point can be predicted by using the prediction model and model parameters.

The relative error used to evaluate the precision of the prediction model is

$$f = \frac{|m|}{W}, \tag{16}$$

where f is the relative error; W is the maximum value; and m is the mean square error, which can be computed by

$$m = \pm\sqrt{\frac{[\Delta\Delta]}{n}}, \tag{17}$$

where Δ is the difference between the measured value and the predicted value; [ ] represents the sum of squares; and n is the number of points involved in calculation.

4.4. Application Scope of the Prediction Model

The lognormal prediction model is a statistical mathematical model that fits in with the skewed curve characteristics. As such, the application of the improved lognormal prediction model is limited. When the movement of the strata above the gob is only affected by self-weight and overburden pressure, the prediction precision of the lognormal prediction model is high. However, when a place has a wide range of geological structure (e.g., faults and folds) or geological events (e.g., earthquakes), the prediction model is unsuitable and the prediction precision is low.

5. RESULTS AND DISCUSSIONS

5.1. In-suit Verification of Skewed Subsidence Characteristics

The measured data of Point A14 was processed, and the development law of the subsidence and subsidence velocity of Point A14 with time was determined (Fig. 7).

The initial, accelerated, decelerated and end subsidence phases of point A14 lasted for 13, 19, 143 and 118 days, respectively. At t = 57, the slope of the subsidence curve is at the maximum and the subsidence velocity reaches the maximum value. The total duration of the initial and accelerated subsidence phases is 32 days, while the total duration of the decelerated and end subsidence phase is 261 days. The total duration of the initial and accelerated subsidence phase is much smaller than the total duration of the decelerated and end subsidence phases. As shown in Figure 7, the subsidence curves of the initial and accelerated subsidence phases are steep whereas those of the decelerated and end subsidence phases are gentle.

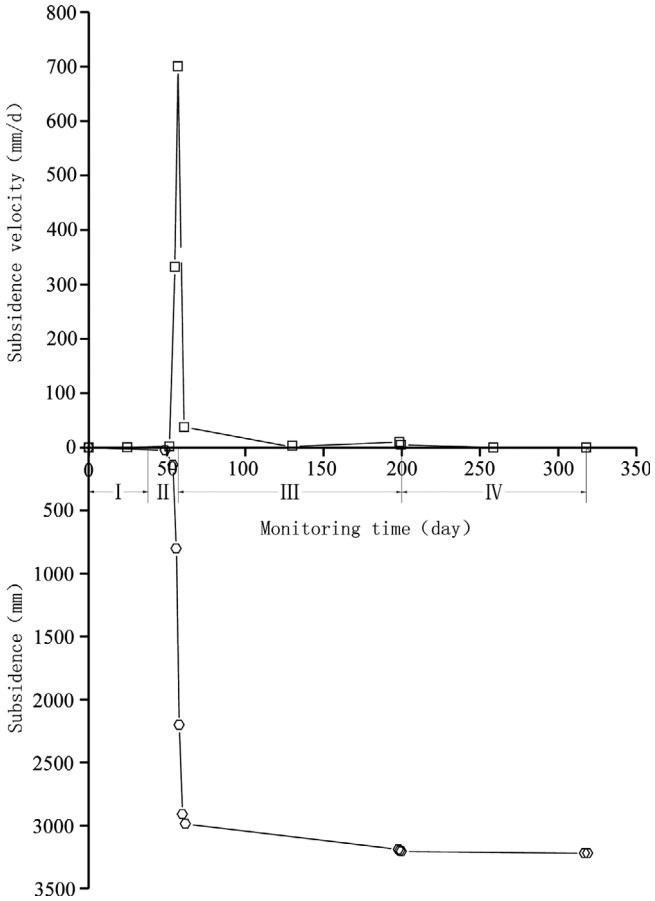

Fig. 7. Movement laws of point A14.

5.2. Model Parameter Acquisition

The normal distribution function was used as reference to analyze the validity of the prediction model. All of the monitoring data of point A14 were used to fit the subsidence prediction model, and the model parameters were obtained. The fitting curve and the model parameters are shown in Figure 8 and Table 2, respectively.

The lognormal distribution fitting equation of the subsidence and the subsidence velocity can be written as

$$w(t) = 3160 \times \left(\frac{1}{2} + \frac{1}{2} \times erf\left(\frac{(\ln(t) - 4.04)}{0.04}\right)\right), \tag{18}$$

$$v(t) = \frac{2918}{0.04\sqrt{\pi}t} \exp\left[-\left(\frac{\ln(t) - 4.04}{0.04}\right)^2\right]. \tag{19}$$

https://doi.org/10.1007/s12303-018-0008-1

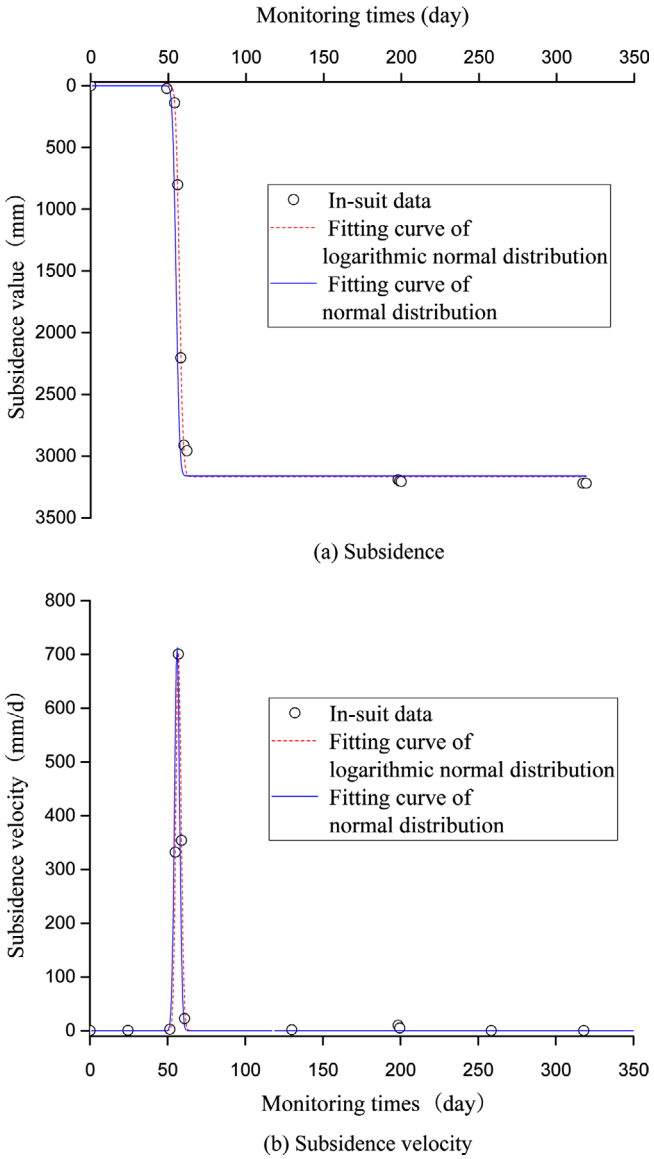

Fig. 8. Fitting curve of observation data of point A14.

The normal distribution fitting equation of the subsidence and the subsidence velocity can be written as:

$$w(t) = 3160 \times \left(\frac{1}{2} + \frac{1}{2} \times erf\left(\frac{(t-56.1)}{2.3}\right)\right), \tag{20}$$

$$v(t) = \frac{2918}{2.3\sqrt{\pi}} \exp\left[-\left(\frac{\ln t - 56.1}{2.3}\right)^2\right]. \tag{21}$$

By using Equations (16) and (17), the fitting root mean square and relative error can be calculated. The fitting result is shown in Table 3.

In the curve fitting process for the subsidence and the subsidence velocity, both normal and lognormal distribution functions exhibited good fitting degrees. However, compared with the normal function, the lognormal distribution function presented a better fitting degree and can better reflect the development law of the subsidence and the subsidence velocity of ground point in the mining-affected area.

5.3. Applicability Analysis of the Skewed Prediction Model

The model parameters were obtained after curve fitting the subsidence and subsidence velocity data of point A14. By taking these parameters into the model, we could then predict the subsidence and subsidence velocity values of the nearby surface monitoring areas (points A12 and A13). By comparing and analyzing the measured value and the predicted value, and according to Formulas (14) and (15), the prediction accuracy of the model was obtained (Table 4).

As shown in Table 4, the prediction accuracy of the lognormal distribution function is better than that of the normal distribution function. The relative error of the lognormal distribution function is slightly higher than 10%, which suggests that the expected precision requirements can be basically met.

Table 2. Model parameters

	Normal distribution		Lognormal distribution	
	Subsidence	Subsidence velocity	Subsidence	Subsidence velocity
w_o	3160	2918	3160	2918
A	56.1	56.1	4.04	4.04
B	2.3	2.3	0.04	0.04

Table 3. Fitting accuracy

	Root mean square		Relative error	
	Normal distribution curve fitting	Lognormal distribution curve fitting	Normal distribution curve fitting	Lognormal distribution curve fitting
Subsidence	282	111	8.9%	3.5%
Subsidence velocity	95	25	13.3%	3.5%

Table 4. Prediction accuracy

		Root mean square		Relative error	
		Normal distribution	Lognormal distribution	Normal distribution	Lognormal distribution
A12	Subsidence	584	434	18.5%	13.7%
	Subsidence velocity	132	75	18.4%	10.5%
A13	Subsidence	458	384	14.5%	12.2%
	Subsidence velocity	147	85	20.5%	11.9%

6. CONCLUSIONS

Establishing the prediction model for surface mining subsidence is vital in mining induced disaster prevention and environmental protection. This work systematically analyzed the skewed subsidence characteristics and constructed the skewed subsidence prediction model. The following are the conclusions.

(1) The rock beam on the side of the gob and the coal pillar exerts different supporting reaction forces. The difference leads to the asymmetry of subsidence velocity, which can form a surface skewed subsidence basin.

(2) The whole movement process of the ground point can be divided into the following stages: initial, accelerated, decelerated and end subsidence phases. The total duration of the initial and accelerated subsidence phase is smaller than that of the decelerated and end subsidence phases.

(3) In this paper, we proposed a new subsidence prediction model that was based on the lognormal function, in which the skewed subsidence characteristics of ground point was considered. The example validated the good prediction accuracy of the proposed model.

ACKNOWLEDGMENTS

This research is supported by the Natural Science Foundation of China (Grant Numbers 51574242, 51774111, 51404272). Those financial supports are gratefully appreciated.

REFERENCES

Bell, F.G., Stacey, T.R., and Genske, D.D., 2000, Mining subsidence and its effect on the environment: some differing example. Environmental Geology, 40, 135–152.

Cui, X.M., Gao, Y.G., and Yuan, D.B., 2014, Sudden surface collapse disasters caused by shallow partial mining in Datong coalfield, China. Natural Hazards, 74, 911–929.

Dai, H.Y. and Wang, J.Z., 2003, Prediction model for surface movement and deformation induced by sub-critical extraction. Journal of China coal society, 28, 583–587.

Dai, H.Y., Zhai, J.C., and Hu, Y.J., 2000, Testing study on the surface displacement of mountainous regions with similar material. Chinese Journal of Rock Mechanics & Engineering, 4, 501–504.

Fan, G.W., Zhang, D.S., and Ma, L.Q., 2011, Overburden movement and fracture distribution induced by longwall mining of the shallow coal seam in the Shendong coalfield. Journal of China University of Mining &Technology, 40, 196–201.

Fan, L.M., Ma, X.D., and Ji, R.J., 2015, The progress of research engineering practice of water-preserved coal mining in western eco-environment frangible area. Journal of China Coal Society, 40, 1711–1717.

He, G.Q., Yang, L., Ling, G.D., Jia, F.C., and Hong, D., 1991, Mining Subsidence Theory. China University of Mining and Technology Press, Xuzhou, 240 p.

Holla, L., 1997, Ground movement due to longwall mining in high relief areas in New South Wales, Australia. International Journal of Rock Mechanics & Mining Sciences, 34, 775–787.

Ju, J.F. and Xu, J.L., 2015, Surface stepped subsidence related to top-coal caving longwall mining of extremely thick coal seam under shallow cover. International Journal of Rock Mechanics and Mining Sciences, 78, 27–35.

Kratzsch, H., 1983, Mining Subsidence Engineering. Springer, Berlin, 537 p.

Liu, B.C., 1982, Introduction of Mining Rock Mechanics. Hunan sciences & technology Press, Changsha, 310 p.

Lu, B.W., Liu, C.W., Liu, D.F., Gao, Y.R., and Wang, Y., 2016, Research on the roof strata moving law in shallow thin bedrock with 3D physical simulation experiment. Journal of Sichuan University (Engineering Science Edition), s1, 107–113.

Luo, Y. and Cheng, J.W., 2009, An influence function method based subsidence prediction program for longwall mining operations in inclined coal seams. Mining Science and Technology, 19, 0592–0598.

Ma, L., Zhang, D., Sun, G., Cui, T., and Zhou, T., 2013, Thick alluvium full-mechanized caving mining with large mining with large mining height face roof control mechanism and practice. Journal of China Coal Society, 38, 199–203.

Peng, S.S., 1978, Coal Mine Ground Control. Wiley, New York, 158 p.

Ramesh, P.S. and Ram, N.Y., 1995, Prediction of subsidence due to coal mining in Raniganj coalfield, West Bengal, India. Engineering Geology, 39, 103–111.

Ren, G., Whittaker, B.N., and Reddish, D.J., 1989, Mining subsidence and displacements prediction using influence functions methods for steep seams. Mining Science and Technology, 8, 235–252.

Sinha, S., Bhattacharya, R.N., and Banerjee, R., 2007, Surface iron ore mining in eastern India and local level sustainability. Resources Policy, 32, 57–68.

 https://doi.org/10.1007/s12303-018-0008-1

Saha, S., Pattanayak, Sk., Sills, Eo., 2011, Under-mining health: environmental justice and mining in India. Health Place, 17, 140–148.

Salmi, E.F., Nazem, M., and Karakus, M., 2017, The effect of rock mass gradual deterioration on the mechanism of post-mining subsidence over shallow abandoned coal mines. International Journal of Rock Mechanics and Mining Sciences, 91, 59–71.

Sasaoka, T., Takamoto, H., Shimada, H., Oya, J., Hamanaka, A., and Matsui, K., 2015, Surface subsidence due to underground mining operation under weak geological condition in Indonesia. Journal of Rock Mechanics and Geotechnical Engineering, 3, 337–344.

Tang, F.Q., 2009, Research on mechanism of mountain landslide due to underground mining. Journal of Coal Science & Engineering, 15, 351–354.

Wang, J.C. and Wang, Z.H., 2015, Stability of main roof structure during the first weighting in shallow high-intensity mining face with thin bedrock. Journal of Mining &Safety Engineering, 2, 175–181.

Wang, J.Z., Kang, J.R., and Chang, Z.Q., 1999, The mechanism analysis on the dissymmetry of the surface subsidence basin. Journal of China coal society, 24, 252–255.

Wang, S.M., Huang, Q.X., and Fan, L.M., 2010, Coal Exploitation and Ecological Water Level Protection in Ecological Fragile Area. Science Press, Beijing, 208 p.

Wang, X.Z., Xu, J.L., Zhu, W.B., and Ju, J.F., 2012, Influence of high mining velocity on periodic weighting during fully-mechanized mining in a shallow seam. Journal of China University of Mining & Technology, 41, 349–355.

Xuan, Y.Q., 2008, Research on movement and evolution law of breaking of overlying strata in shallow coal seam with a thin bedrock. Rock and Soil Mechanics, 29, 512–516.

Yu, B., Zhao, J., Kuang, T.J., and Meng, X.B., 2015, In situ investigations into overburden failures of a super-thick coal seam for longwall top coal caving. International Journal of Rock Mechanics and Mining Sciences, 78, 155–162.

Zhang, J. and Chong, L., 2012, The discussion of the surface and building deformation in the coal mining subsidence area. Shanxi Architecture, 38, 83–84.